Available online at www.sciencedirect.com
SCIENCE DIRECT®
Journal of Nuclear Materials 329–333 (2004) 706–710
journal of nuclear materials
www.elsevier.com/locate/jnucmat

Formation of dust particles under the influence of intense thermal loads

Y. Koza *, E. Berthe, E. Lehmann, J. Linke, M. Rödig, E. Wessel, L. Singheiser

Forschungszentrum Jülich GmbH, EURATOM Association, Institüt fur Werkstoffe und Verfahren der Energietechnik, D-52425 Jülich, Germany

Abstract

Intense thermal loads in fusion devices which occur during ELMs (edge localized modes), plasma disruptions and VDEs (vertical displacement events), will result in macroscopic erosion associated with the formation of cracks, droplets, evaporation, and melting, or sublimation. A fraction of dust particles will sublimate in the boundary plasma; others may be deposited in gaps and shadowed areas of the divertor region. Tritium uptake in these particles will be a critical issue in future thermonuclear fusion devices. Evaporation and the formation of tungsten droplets induced by boiling of tungsten may result in a severe contamination of the boundary plasma. In order to simulate the effect of dust formation under transient heat fluxes, heat load tests have been performed in the electron beam test facility JUDITH on tungsten and carbon based materials.

1. Introduction

During steady state operation and off-normal events, high thermal energy will be deposited on the plasma facing components and cause degradation of the plasma facing materials. Especially during intense transient thermal loads such as ELMs (edge localized modes), plasma disruptions, and VDEs (vertical displacement events), irreversible damage might occur [1,2]. For carbon based materials crack formation, dust generation, and sublimation are the main erosion mechanisms [3,4]. Brittle destruction [5] associated with sublimation and emission of solid particles caused by transient thermal loads leads for dust formation and macroscopic erosion [6]. Carbon dust has a high affinity for the formation of hydrocarbons with tritium; hence, the resulting large tritium inventory is a serious safety concern [7].

For refractory metals like W, ablation, crack and droplet formation, and melting are major erosion processes which limit the lifetime of the components [2,8]. In particular, the dust formation of W associated with evaporation and droplet formation is a radiological safety issue because neutron irradiated tungsten is highly radioactive.

In this paper, intense transient thermal load experiments were performed under the condition of ELMs, plasma disruptions, and VDEs in an electron beam facility with energy densities of 1–60 MJ m^{-2} and pulse durations of 0.5–90 ms for carbon and high-Z materials. The effect of elevated temperatures around DBTT were also studied.

2. Experimental

The carbon based materials used in this study are isotropic fine grain graphite (R6650) by Ringsdorfwerke, Germany, 3 directional carbon fiber composites (3D-CFC) NB31, and Si-doped 3D CFC NS31 by SNECMA Propulsion Solide, France. The metal samples used for the campaign are, W, Mo, Ta, plasma sprayed (PS) W, and W alloys (W–1%La_2O_3, W–26%Re). The typical sample dimensions are $12\times12\times5$ mm^3 for disruption and $25\times25\times10$ mm^3 for ELM and VDE tests.

* Corresponding author. Tel.: +49-2461 616300; fax: +49-2461 613699.
E-mail address: y.koza@fz-juelich.de (Y. Koza).

0022-3115/$ - see front matter © 2004 Published by Elsevier B.V.
doi:10.1016/j.jnucmat.2004.04.187

Simulation experiments were performed in the electron beam test facility JUDITH. A fast beam scanning with frequencies of $f_x = 46.5$ kHz and $f_y = 43.4$ kHz has been applied to get a homogeneously loaded area under plasma disruption and VDE tests. Simulation experiments with ELM-specific thermal loads were performed with a stationary beam. For the above mentioned experiments the beam width has been determined by calibration tests using different calorimeters. The focus of the beam in the stationary loading was optimized resulting in a beam width FWHM (full width at half maximum) = 1.84 mm. The typical loading conditions were chosen as follows: 1 MJ m^{-2} at a pulse duration $\Delta t = 0.5$ ms for ELMs, 5–7 MJ m^{-2} for disruption tests ($\Delta t = 4$–5 ms), and 60 MJ m^{-2} for VDE tests ($t = 90$ ms).

For diagnostics during thermal load tests an oscilloscope and a CCD camera were applied to measure the absorbed current, the pulse duration, and to detect the emission of the particles. Characterization of the test materials was carried out using microscopy (optical, SEM), laser profilometry, and metallography.

3. Results

3.1. Particle emission

The onset of particle emission from graphite under intense transient thermal loads was determined by systematic experiments using digitized camera images [6]. Fig. 1 shows that off-normal events such as plasma disruptions and VDE conditions are in the regime above the threshold (dashed line) and cause catastrophic damage due to brittle destruction (BD) [5] even after single electron beam pulses. Under these conditions the resulting weight loss was up to 0.3 mg per pulse and the erosion depth in the range from 10 to 80 μm [6,9]. The expected loading conditions for ELMs in ITER condition are well below the threshold curve. However, ELMs will occur during normal plasma operation with a frequency of ≈1 Hz which integrates to >10^6 events during the lifetime of the components in ITER [1]. Therefore, the material degradation due to high cycle thermal fatigue has to be investigated.

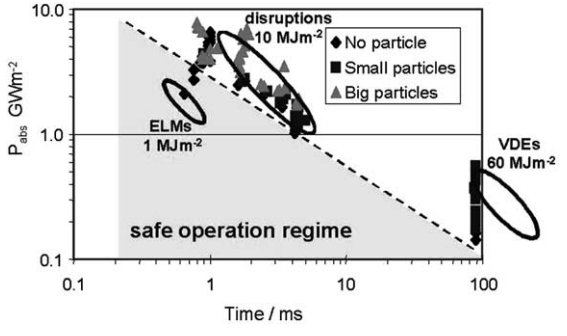

Fig. 1. Threshold for the onset of particle emission from fine grain graphite.

Although CFCs have a completely different microstructure from graphite, both materials show intense BD-effects which are associated with the release of small (primarily binder phase or matrix material) and large particles (graphite grains, carbon fiber segments, grain or fiber clusters). The better thermal conductivity values of the fiber reinforced graphite have only minor influence on the threshold level for the onset of particle emission. For Si-doped CFCs (NS31) the threshold is shifted slightly to lower power density levels. Different from the undoped carbon materials, the Si-doped CFC also generated droplets of molten silicon [6,10].

Surface melting and the removal of the melt layer during transient heat load conditions is a serious concern for all metallic plasma facing materials. To investigate this effect on refractory metals under disruption specific thermal loads a systematic experiment was performed on test specimens made from sintered tungsten. In these test the incident current I_{inc} was increased from 40 to 320 mA (increment $I_{inc} = 40$ mA, $U_{acc} = 120$ kV) for pulse duration of 5 ms. Fig. 2 shows the surface morphologies together with the released particles which were monitored by a digital camera for absorbed energy densities of 3.2, 6.2 and 10.4 MJ m^{-2} (corresponding to $I_{inc} = 80$, 160, and 280 mA). For $I_{inc} < 80$ mA there is only negligible particle emission. Above this level clear emission of particles was observed; the intensity and the brightness of the particle trajectories increase with the beam current (Fig. 2(A)). Under these condition the loaded surface does not show any melting. Evidence of a clear melt crater was found at an incident beam current of 160 mA (Fig. 2(B)), i.e. well above the onset of the particle emission process. Hence, tungsten surfaces exposed to 5 ms beam pulses below the melting threshold are a source for hot or molten W dust particles; the particle release may be associated with a BD-process in analogy to the carbon based materials.

The major fraction of the particle trajectories which are emitted for $I_{inc} \geqslant 240$ mA consist of two separate segments (Fig. 2(C)): first a faint thin line with decreasing intensity, and a second one which is associated with a strong increase in the particle brightness after traveling a distance of ≈1–7 cm. Other materials such as carbon based materials and other metals with lower melting points always showed continuous emission lines [9]. Up to now there is no clear explanation for the existence of two separate intensities of the trajectories. A phase change from liquid to solid in the particle surface is the most likely explanation. The existence of a dense, absorbing vapor cloud could be another cause.

For medium energy densities (e.g. $E_{abs} = 6.2$ MJ m^{-2}) there is only negligible ejection of the liquid melt layer

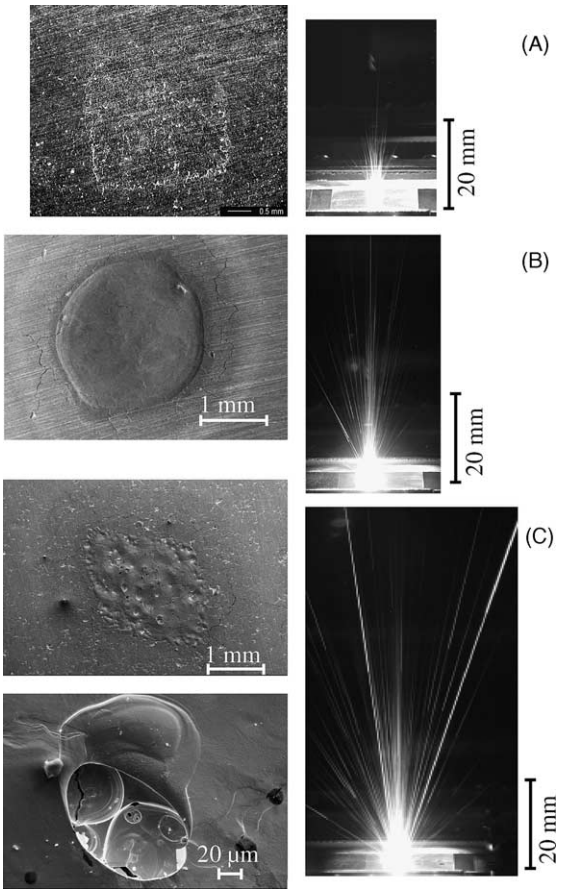

Fig. 2. Surface morphologies (left column) and digital images (right column) of pure sintered W samples during transient electron beam loading. (A) $I_{Inc} = 30$ mA, $E_{abs} = 3.2$ MJ m^{-2}, $\Delta t = 4.1$ ms; (B) $I_{inc} = 160$ mA, $E_{abs} = 6.2$ MJ m^{-2}, $\Delta t = 4.4$ ms; (C) $I_{inc} = 280$ mA, $E_{abs} = 10.4$ MJ m^{-2}, $\Delta t = 4.4$ ms.

from the heated area; nevertheless, a clear erosion crater is formed due to the high vapor pressure which tends to eject the melt outside the loaded area (Fig. 2(B)). With increasing beam current an additional process, intense convection of melt layer occurred and partially boiling of the melt has been observed (Fig. 2(C)). Obviously some local spots were overheated exceeding the boiling temperature of tungsten. Impurities might also provoke the formation of bubbles. These processes might be the source for an additional release of liquid W particles.

3.2. Degradation of refractory metals

To compare the resistance of different refractory metals under disruption heat loads, a selection of high-Z materials (Mo, Ta, W–1%La_2O_3, W–26%Re, PS-tungsten) have been subjected to single 5 ms electron beam pulses at $E_{abs} \approx 6$ MJ m^{-2} (cf. Figs. 2(B) and 3). The resulting erosion crater in pure sintered tungsten (Fig. 2(B)) shows a slight displacement of the melt layer due to the arising vapor pressure. This also applies to other high-Z materials (Fig. 3(A)–(D)), however, the depression of the meniscus increases with the vapor pressure of the material, e.g. in the La_2O_3-doped tungsten. Probably La_2O_3 starts to evaporate after 1 ms according to the sudden drop of the absorbed current which was not observed in pure W samples. This vapor deforms the molten area causing convection of the melt layer which finally results in the formation of a rough resolidified surface. Since tungsten is rather brittle below DBTT (ductile brittle transient temperature), significant crack formation has been observed at the periphery of the melt crater for the pure sintered tungsten (Fig. 2(B)). Intense cracks have been detected in W–1%La_2O_3 samples at identical heat loads. Some of these cracks which follow the texture of the rolled material are clearly visible (even in the melt crater, Fig. 3(A)). Since these cracks are oriented perpendicular to the surface, they do not form a thermal barrier and the substrate rarely ablates. On the other hand, these cracks might become critical because they can easily penetrate to the heat sink or water channel. The depth of these cracks extends several millimeters into the bulk material. W–26%Re shows some gradual improvement (Fig. 3(B)). Other refractory metals such as molybdenum or tantalum do not develop any remarkable cracks (Fig. 3(C) and (D)).

Clear evidence for the formation of large droplets of molten tungsten has only been found on PS coatings

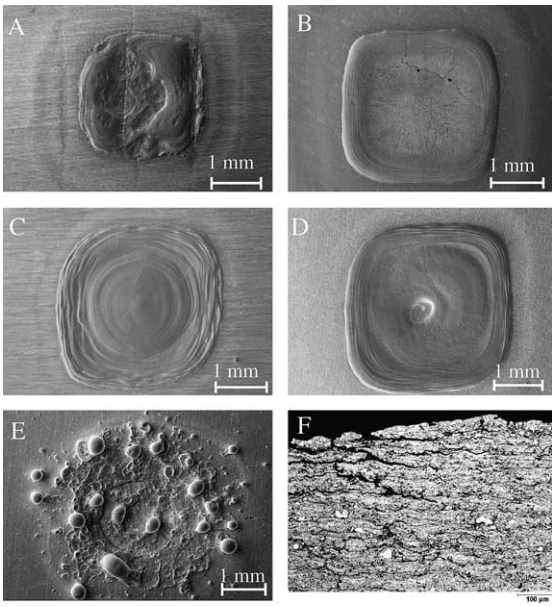

Fig. 3. SEM micrographs of W–1%La_2O_3 (A), W–26%Re (B), molybdenum (C), tantalum (D), and plasma sprayed W on Cu (E–F) following electron beam tests with an absorbed energy density $E_{abs} = 5$–7 MJ m^{-2} ($I_{inc} = 160$ mA, $\Delta t = 4.4$ ms).

(Fig. 3(E) and (F)). The porosity of these coatings and the microstructure with elongated splats are the main reasons for a reduced thermal conductivity; hence overheating of the melt layer and boiling effects become essential at lower incident energy densities in comparison to monolithic sintered tungsten. The trajectories from emitted particles originating from PS-tungsten coatings are characterized by bright curved traces which suggests the creation of heavy droplets moving at a relatively low speed. The crack growth between the individual splats (Fig. 3(F)) and the subsequent detachment from adjacent layers may be another possible source for the generation of tungsten dust particles.

The simulation of VDEs has been performed with longer beam pulses ($\Delta t \approx 100$–300 ms); the absorbed energy density was $E_{abs} \approx 60$ MJ m^{-2} according to the ITER requirements. Typical examples for 90 ms tests on pure tungsten are shown in Fig. 4 both for a monolithic and a lamella-type structure. The lamella-type heat flux component which consists of thin-stacked tungsten lamellae with 200 μm thickness each lamella HIPed to CuCrZr tube [10]. Under VDE conditions the resulting melt layer forms a relatively deep crater with a marked rim. There are no indications for the formation of large droplets for the sintered tungsten sample. However, the lamella-structure (Fig. 4(B)) shows stronger melting and clear evidence of melt droplets; this may be due to the barrier effect of the gaps between the individual lamellae and thus the lower effective thermal conductivity of this test specimen. On the other hand, the intense crack formation outside the heat affected area in sintered tungsten has been completely suppressed in the lamella-structure. Monolithic test sample preheated to 500 °C (T > DBTT) did not show any crack formation outside the loaded area.

Due to the intense evaporation during transient thermal exposure, a dense cloud of ablation vapor will form above the heat affected area. Since W has a high reflection coefficient, about 47% of the incident electrons are reflected and will ionize the ablation vapor. In future confinement experiments such as ITER this vapor cloud will also contribute to a partial shielding of the incident particles and mitigate the material damage during severe disruptions [11].

Erosion depths measurements on electron beam simulated plasma disruptions also indicate a shielding effect. The erosion depth for bulk and PS-tungsten as a function of the absorbed power density is shown in Fig. 5; the measured data show a clear minimum for power densities of about 1.6 GW m^{-2} (corresponding to an energy density of ≈8MJ m^{-2}). Shielding effects have also been reported from electron beam tests on carbon based materials for intense 1 ms electron beam pulses [6].

Simulation experiments of ELMs for low cycle numbers were carried out at maximum energy density $E_{abs} = 1.2$ MJ m^{-2} for pulse duration of 0.52 ms using a non-scanned beam ($I_{inc} = 150$ mA, $V = 120$ kV).

After a single shot slight particle emission has been detected with the CCD camera. Surface analysis by SEM methods shows clear melting in the e-beam affected surface area. In addition, metallographic analyses show

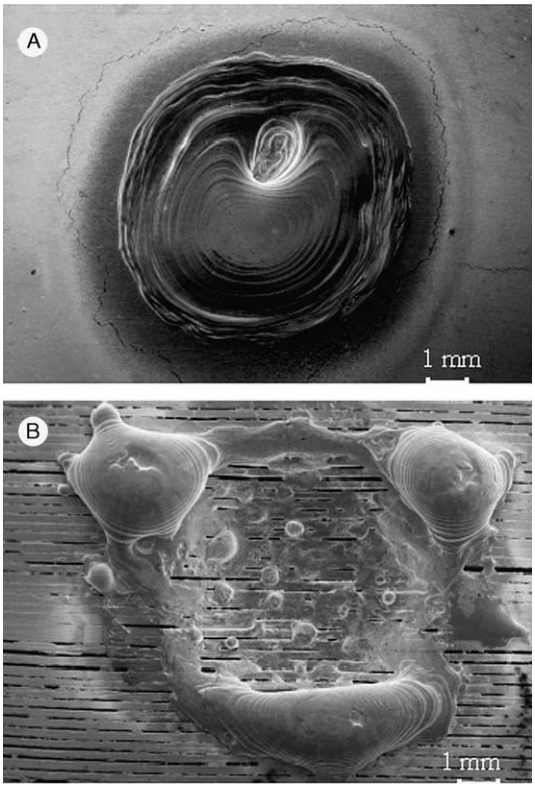

Fig. 4. SEM images of pure W; bulk (A) and 0.2 mm lamellae (B). (A) $E_{abs} = 53$ MJ m^{-2}, $I_{inc} = 320$ mA, $\Delta t = 89$ ms; (B) $E_{abs} = 59$ MJ m^{-2}, $I_{inc} = 320$ mA, $t = 89$ ms.

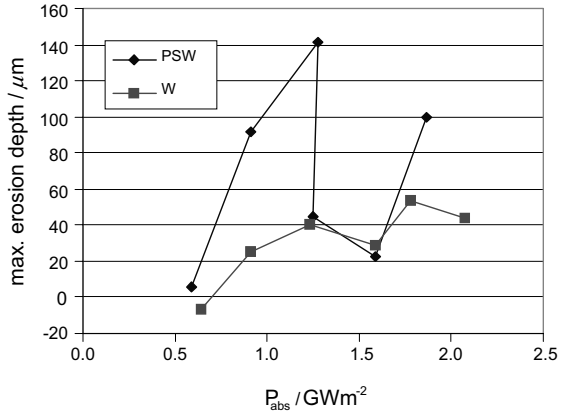

Fig. 5. Variation of erosion depth with absorbed power density P_{abs} of pure W and plasma sprayed W coating (PS-W) ($\Delta t = 4.2$–4.5 ms).

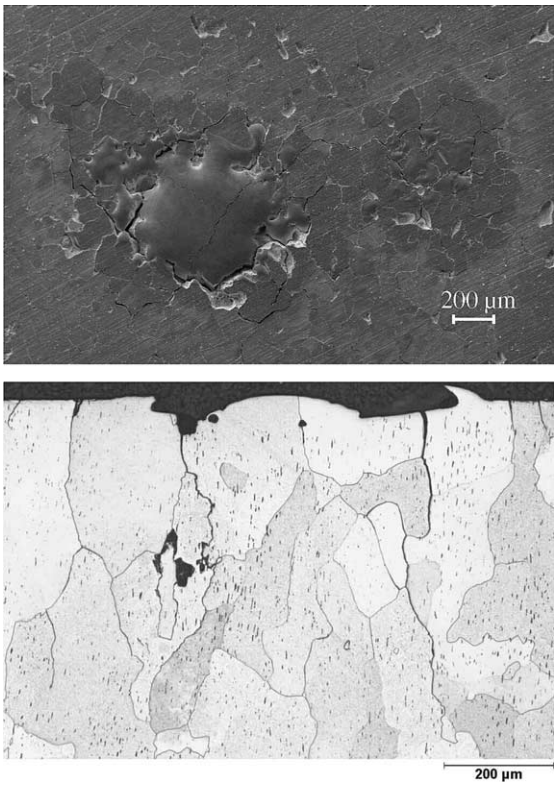

Fig. 6. SEM (top) and cross section (bottom) images of W subjected to ELM conditions for low cycle numbers. $I_{inc} = 150$ mA, $U_{acc} = 120$ keV, $\Delta t = 0.52$ ms, $E_{abs,max} = 1.2$ MJ m^{-2}; number of pulses $n = 100$.

several cracks perpendicular to the surface with a depth of 50–200 μm; some intersected W-grains in the sample surface are missing. After 100 cycles the trajectories of emitted particles were not detected and a convex melt layer has been formed; the metallography shows a few bubbles in the recrystallized material and several cracks around the crater with a depth up to ≈500 μm (Fig. 6). Obviously the cracks in the vicinity of the melt spot play an important role for the thermal isolation of the adjacent substrate and for an accelerated local heating and evaporation of the heat affected area. The crater depth of W after a single ($d = 38$ μm) and after 100 shots ($d = 27$ μm) did not show a big difference.

4. Conclusions

Dust formation under intense transient thermal loads has been studied for carbon based materials and refractory metals for thermal loads which are representative for plasma disruption, VDEs, and ELMs in next step fusion devices such as ITER. In graphites and CFCs the major mechanism for the generation of dust is brittle destruction; in particular for short events in the ms-range with very high energy densities.

For high-Z metals melt layer ejection and boiling effects are the main source for the formation of (neutron activated) W dust particles; the extent of the resulting material damage depends strongly on the applied thermal loads, the material parameters and the prevailing temperature. For ITER specific transient loads melting of the heat affected surface is essential for all transient events considered in this work: disruptions, VDEs, and ELMs. Due to the absence of strong electromagnetic forces in electron beam simulation tests, a catastrophic ejection of the melt layer does not occur. However, enhanced erosion scenarios initiated by strong evaporation and/or boiling processes have been observed during disruptions and VDEs, in particular

- with increasing power density of the incident beam,
- for high-Z materials with reduced thermal conductivity (e.g. PS-tungsten),
- for materials with higher vapor pressure,
- test samples with internal thermal barriers (e.g. lamellae).

The resulting material erosion may be affected by vapor shielding effects, both in fusion devices or in high heat flux simulation experiments. Apart from material erosion the formation of cracks is another serious effect with strong impact on the lifetime of the components. Here significant improvements are possible if more ductile materials or alloy are utilized; castellation, lamellae-type structures and operation above DBTT are additional important measures to avoid crack initiation.

References

[1] G. Federici et al., Fus. Eng. Des. 61&62 (2002) 81.
[2] M. Merola et al., J. Nucl. Mater. 258–263 (1998) 653.
[3] V. Safronov et al., J. Nucl. Mater. 290–293 (2001) 1052.
[4] M.I. Guseva et al., Fus. Eng. Des. 66–68 (2003) 389.
[5] H. Würz et al., J. Nucl. Mater. 307–311 (2002) 60.
[6] J. Linke et al., Fus. Eng. Des. 66–68 (2003) 395.
[7] M.F. Stamp et al., Phys. Scr. T 91 (2001) 13.
[8] A. Makhankov et al., J. Nucl. Mater. 290–293 (2001) 1117.
[9] Y. Koza et al., Phys. Scr., to be published.
[10] M. Rödig et al., Fus. Eng. Des. 61&62 (2002) 135.
[11] A. Hassanein, I. Konkashbaev, J. Nucl. Mater. 283–287 (2000) 1171.